# Optimizing the Design of a Rijke Tube Experiment for Combustion Stability Model Identifiability

Xiaoling Chen, Evan Dillen, Hosam Fathy, and Jacqueline O'Connor<sup>1</sup>

Abstract—This paper presents the design of a thermoacoustically unstable combustor experiment for identifiability. We examine the impact of sensor placement, flame location, and acoustic excitation frequency on the Fisher identifiability of a one-dimensional combustion stability model's parameters. The model uses linear delay differential equations to describe both the acoustics and heat release dynamics in a laboratory combustor called a Rijke tube. We derive analytic expressions for the frequency-domain Fisher identifiability of the model's parameters. This leads to two key insights. First, excitation frequency, flame location, and sensor placement all have a significant impact on parameter identifiability. Second, the optimal excitation frequencies for identifiability are not strong functions of sensor placement but change with flame location. Building on these insights, the paper concludes by using a genetic algorithm to optimize the design of a Rijke tube experiment for thermoacoustic model identifiability.

### I. INTRODUCTION

This paper examines two main questions. First, how accurately can one estimate the parameters of a thermoacoustic combustion stability model from laboratory data? Second, to what extent is it possible to improve this accuracy through optimal experimental design? The paper focuses on a linear, physics-based, one-dimensional model of a common laboratory combustor known as a "Rijke tube" [1].

Our research is motivated by the challenge of combustion instability in lean premixed commercial gas turbines and the potential of model-based active control to address this challenge. Combustion instability is an operational risk in systems such as gas turbines, furnaces, and rocket engines [2]. It arises from the coupling between acoustic pressure and unsteady heat release rate fluctuations in the flame. Depending on the phase difference between the fluctuations of heat release rate and pressure, this coupling can create a positive feedback loop, thereby inducing instability. The resulting high-amplitude pressure oscillations can cause significant damage to the combustor hardware. This consequence is undesirable and increasingly problematic as the power generation industry migrates towards lean premixed combustion techniques that provide lower emissions at the expense of greater vulnerability to instability.

The literature presents both passive and active techniques for attenuating or perhaps eliminating combustion instability. Passive control methods include the modification of combustor geometries [3], implementation of acoustic dampers [4], and fuel staging [5]. The main idea behind active combustion instability control is to utilize an external actuation signal,

such as fueling or acoustic excitation, in order to break the positive feedback coupling between heat release and acoustic oscillations ([6], [7], [8], [9]). Active controllers can be designed using either empirical [10] or model-based methods. They have been shown to be promising in the laboratory, but to the best of the authors' knowledge, they have only been fielded on one industry-scale engine [11].

The effectiveness of a model-based active stability controller depends on the accuracy with which the underlying combustion dynamics are modeled and parameterized. The literature presents a number of studies on the application of both physics-based and empirical modeling/identification techniques to the combustion stability problem (e.g., [12], [13], [14], [15]). However, to the best of the authors' knowledge, the critical challenges of uncertainty quantification and experimental design optimization for combustion stability modeling remain relatively unexplored. In particular, there is a need for in-depth analyses of the statistical accuracy with which combustion stability models can be parameterized from a given experiment. Moreover, there is a need for optimizing the design of lab experiments to achieve better combustion stability parameter estimation accuracy. One common combustion stability experiment involves measuring the response of a local pressure signal inside a combustion chamber to acoustic excitation in the frequency domain. Key questions when designing such an experiment include the following: where should the pressure sensors be placed relative to the flame location, and what excitation frequencies should be used for parameter estimation?

The goal of this paper is to address the above research challenges. Specifically, the paper utilizes Fisher information analysis to assess the accuracy with which the parameters of a linear time-delay combustion model can be estimated from experimental data. The specific parameters of interest are an amplification factor and a time delay relating the rate of heat release at the flame to combustor acoustic oscillations [16]. Both parameters can be measured experimentally [17]; our goal in this paper is the assessment and optimization of their estimation accuracy. We perform the uncertainty quantification portion of this work using Fisher information analysis. Moreover, we examine and optimize the impact of three key experimental design parameters on Fisher identifiability, namely: sensor placement, flame location, and acoustic excitation frequency. Fisher information is an established means for such uncertainty quantification/optimization [18], [19], [20], [21], [22]. It is well-suited for assessing the local identifiability of a model's parameters around a nominal value, which is useful in the context of this work, given

<sup>&</sup>lt;sup>1</sup>Authors are with the Department of Mechanical Engineering, Pennsylvania State University, University Park, PA 16802, USA jxo22@psu.edu

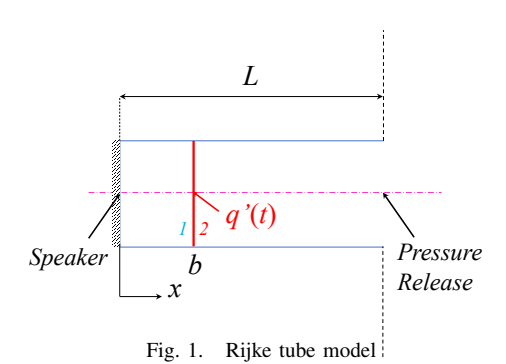
the degree to which the existing literature already provides nominal estimates of the above model parameters [17].

The remainder of this paper is organized into three main parts, focusing on introducing the paper's combustion stability model (Section II), analyzing its parameter identifiability (Section III), and optimizing this identifiability through experimental design (Section IV). The paper concludes by summarizing the results of this analysis and optimization.

### II. PROBLEM FORMULATION

### A. Rijke Tube Configuration

Fig.1 shows a Rijke tube of length L. On the left boundary lies an acoustic excitation source. The Rijke tube's right boundary is exposed to atmospheric pressure,  $p_{atm}$ , generating a pressure release boundary. Fuel and air mixtures flow in positive x direction (i.e., left to right) at a low Mach number. An acoustically-compact flame sits at x = b,



#### B. Thermoacoustic Model

We assume an isentropic, homogeneous, and steady mean flow as well as a step temperature rise across the flame in the Rijke tube. Following the work of Dowling and Stow [2], we obtain linearize continuity, momentum, and energy conservation equations for the thermoacoustic system. These equations assume that: (i) the mean flow occurs at a small Mach number (*i.e.*, the bulk flow velocity  $u_b$  is low); and (ii) fluctuations in density, pressure, velocity, and temperature around equilibrium states are small. The resulting linearized conservation equations for the one-dimensional thermoacoustic model in space x and time t are:

$$\frac{\partial \rho'}{\partial t} + \bar{\rho} \frac{\partial u'}{\partial x} = 0, \ \bar{\rho} \frac{\partial u'}{\partial t} = -\frac{\partial p'}{\partial x} \tag{1}$$

$$\frac{\partial p'}{\partial t} = -\bar{\rho}\bar{c}^2 \frac{\partial u'}{\partial x} + (\gamma - 1)q', \tag{2}$$

where,  $\bar{c}$  and  $\bar{\rho}$  represent the speed of sound and density, respectively. Oscillations of pressure, density, particle velocity, and heat release rate per unit volume are denoted by p',  $\rho'$ , u' and q'. The coefficient in front of q' includes the specific heat ratio  $\gamma$ . We assume a linear time-lag model (n- $\tau$  model), as indicated in (3), to govern the heat release rate response of the compact flame per unit cross sectional area

Q'. In this model,  $\beta$  is the amplification factor,  $\tau$  is the time delay, and  $u'_1$  is the particle velocity oscillation just upstream the flame. The equivalent amplification factor n is obtained based on (4), where  $c_{p,1}$  is the constant pressure specific heat of premixed fuel and air, and  $\Delta T$  is the temperature rise across the flame.

$$q'(x,t) = Q'(t)\delta(x-b), \ Q'(t) = -\frac{\beta\bar{\rho}\bar{c}^2}{\gamma - 1}u'_1(t-\tau)$$
 (3)

$$n = \left| \frac{Q'(t)/\bar{Q}}{u'(t)/\bar{u}} \right| = \left| -\frac{\beta \bar{c}_1^2}{\gamma - 1} \frac{1}{c_{p,1} \Delta T} \right| \tag{4}$$

Equation (5) includes the two boundary conditions (B.C.s) shown in Fig.1. The speaker provides acoustic forcing with particle velocity oscillations  $u'_0(t)$  at the Rijke tube's closed end; the other end is open to atmospheric pressure, creating a pressure release boundary condition.

$$u'(0,t) = u'_0(t), \ p'(L,t) = 0$$
 (5)

Based on the above equations, we derive a thermoacoustic wave equation in (6). The mean variables are constant in the regions upstream and downstream of the flame and  $p_1'$  is the pressure oscillation located just upstream the flame,  $x = b^{-}$ .

$$\frac{\partial^2 p'}{\partial t^2} - \bar{\rho}\bar{c}^2 \frac{\partial}{\partial x} \left( \frac{1}{\bar{\rho}} \frac{\partial p'}{\partial x} \right) = \frac{\beta \bar{\rho}\bar{c}^2}{\bar{\rho}_1} \delta(x - b) \frac{\partial p'_1(t - \tau)}{\partial x}$$
 (6)

#### C. Solution to Thermoacoustic Model

Since the thermoacoustic model is linear, We apply the Laplace transform to equation (6) with the zero initial conditions in (7). The transformed  $2^{\text{nd}}$ -order ordinary differential equation in the frequency-domain s is in (8).

$$p'(x,0) = 0 \tag{7}$$

$$\frac{s^2}{\bar{\rho}\bar{c}^2}P'(x,s) - \frac{d}{dx} \left[ \frac{1}{\bar{\rho}} \frac{dP'(x,s)}{dx} \right] \\
= \frac{\beta e^{-\tau s} \delta(x-b)}{\bar{\rho}_1} \frac{dP'(x,s)}{dx} \Big|_{x=b^-}$$
(8)

The two boundary conditions in time domain correspond to the two boundary conditions in the *s*-domain in (9). Additionally, we apply two B.C.s across the flame: (i) a continuity pressure oscillation p' in (10); and (ii) a relation of the first-order spatial derivative of P' between regions upstream and downstream flame from the integration of (8) over the flame region [ $b^-$ ,  $b^+$ ] in (11).

$$U'(0,s) = \mathcal{L}\{u'_0(t)\} = U'_0(s), \ P'(L,s) = 0$$
 (9)

$$P'(b^-, s) = P'(b^+, s) \tag{10}$$

$$\frac{dP'(x,s)}{dx}\Big|_{x=b^{+}} = (1 - \beta e^{-\tau s}) \frac{\bar{\rho}_{2}}{\bar{\rho}_{1}} \frac{dP'(x,s)}{dx}\Big|_{x=b^{-}}$$
(11)

We solve for the distribution of pressure oscillation P'(x,s) along the Rijke tube's axial coordinate for regions upstream and downstream of the flame in (12) and (13) separately. Appendix A includes the new variables definitions in (27).

$$P'(x,s) = \bar{\rho}_1 \bar{c}_1 U_0'(s) \frac{(\bar{\rho}\bar{c}e_{24})e^{-\frac{x}{\bar{c}_1}s} - (\bar{\rho}\bar{c}e_{13})e^{\frac{x}{\bar{c}_1}s}}{\bar{\rho}_m \bar{c}_m e_m + \bar{\rho}_n \bar{c}_n e_n}$$
(12)

$$P'(x,s) = -\frac{(\bar{\rho}_m^2 \bar{c}_m^2 - \bar{\rho}_n^2 \bar{c}_n^2) e^{t_5 s} U_0'(s)}{2(\bar{\rho}_m \bar{c}_m e_m + \bar{\rho}_n \bar{c}_n e_n)} \left( e^{\frac{x}{\bar{c}_2} s} - e^{\frac{2L - x}{\bar{c}_2} s} \right)$$
(13)

### D. Transfer Function

In this Rijke tube setup, the actuator input is the acoustic excitation from a speaker mounted at the combustor inlet. The output is the local pressure oscillation measured at one location along the Rijke tube. Considering the different units of the input and output, we define a normalized transfer function based on the dimensionless input and output in (14). The nominal pressure is atmospheric pressure  $p_{atm}$  and the nominal velocity is bulk flow velocity  $u_b$ .

$$H_n(x,s) \equiv \frac{P'_n(x,s)}{U'_n(s)}$$

$$P'_n(x,s) = \frac{P'(x,s)}{p_{atm}}, \ U'_n(s) = \frac{U'_0(s)}{u_b}$$
(14)

Similar to the pressure distribution, the transfer function has different forms in the regions upstream and downstream of the flame, displayed in (15) and (16). Knowing the flame location at x = b and mean heat release rate, we obtain the spatial distribution of the mean variables. For fluctuating variables, the flame dynamics describing the dependence of the heat release rate fluctuations on acoustic velocity oscillations contain the amplification factor  $\beta$  and time delay  $\tau$ , which significantly affect the transfer function characteristics. Additionally, the transfer function depends on sensor placement  $x_0$  and acoustic forcing frequency  $\omega = s/j$ . In one example under conditions specified in Table I, the transfer function magnitude response is plotted in Fig.2. The high magnitude peaks of the transfer function correspond to the first three longitudinal acoustic resonant modes of the thermoacoustic system.

Fig.2 displays the frequency response of the normalized transfer function magnitude  $|H_n(x,s)|$  observed at four locations along the Rijke tube, including locations both upstream and downstream of the flame. The four sensors all observe the first three longitudinal acoustic modes of this one-dimensional combustor, corresponding to one quarter-, three quarters-, and five quarters-longitudinal modes.

$$H_n(x,s) = \frac{\bar{\rho}_1 \bar{c}_1 u_b}{p_{atm}} \frac{(\bar{\rho} \bar{c} e_{24}) e^{-\frac{x}{\bar{c}_1} s} - (\bar{\rho} \bar{c} e_{13}) e^{\frac{x}{\bar{c}_1} s}}{\bar{\rho}_m \bar{c}_m e_m + \bar{\rho}_n \bar{c}_n e_n}$$
(15)

$$H_n(x,s) = -\frac{(\bar{\rho}_m^2 \bar{c}_m^2 - \bar{\rho}_n^2 \bar{c}_n^2) e^{t_5 s} u_b}{2p_{atm}(\bar{\rho}_m \bar{c}_m e_m + \bar{\rho}_n \bar{c}_n e_n)} \left(e^{\frac{x}{\bar{c}_2} s} - e^{\frac{2L - x}{\bar{c}_2} s}\right)$$
(16)

 $\label{eq:TABLE I} \mbox{\sc Parameter Specification of Rijke Tube Combustion}$   $\mbox{\sc Instability Model}$ 

Parameter Name	Symbol	Value	Unit
Rijke tube length		1	m
Flame location	b	0.25	m
Temperature upstream flame	$T_1$	288.15	K
Mean bulk flow velocity	$u_{\rm b}$	5	m/s
Temperature rise across flame	$\Delta T$	1900	K
Specific gas constant	R	287	J/kgK
Specific heat capacity ratio	$  \gamma  $	1.4	-
Atmospheric pressure	$p_{atm}$	$1.013 \times 10^{5}$	Pa
Particle velocity amplitude from acoustic forcing	$\hat{u}_0$	1	m/s
Amplification factor	β	0.5	-
Amplification factor	n	0.0758	-
Time delay	$\tau$	2.0	ms

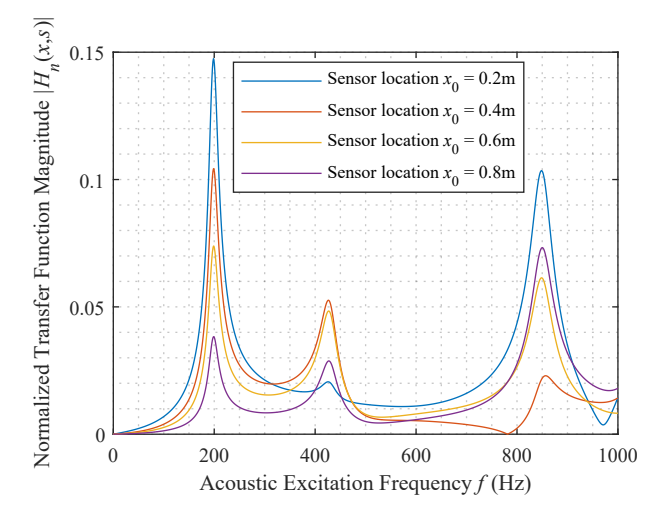


Fig. 2. Transfer function frequency response with model specifications in Table I at four sensor placements

### E. Transfer Function Magnitude Comparison to Time-Domain Simulation

To see if the frequency-domain based model derived in section II-D captures the open-loop system characteristics, we conduct a time-domain simulation with the same input and output as the frequency-domain model by applying the open source combustion instability low order simulator (OSCILOS) developed by Li et al. [23]. The particle velocity oscillation is the input driven by a speaker at Rijke tube inlet,  $x_0 = 0.0 \, m$ , and the sensors observe the output pressure oscillation at two locations,  $x_0 = 0.2 \, m$  and 0.4 m. Based on input and output time series, we apply cross-spectral analysis to calculate the transfer function magnitude between the two signals [15]. Fig.3 illustrates the the transfer function magnitude comparisons between the frequency- and time-domain modeling, showing a good agreement at nearly all frequencies for the two sensor placements.

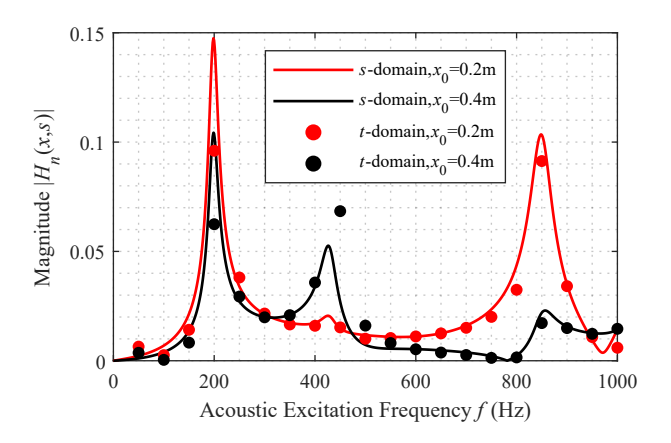


Fig. 3. Transfer function frequency response comparisons between frequency domain modeling and time domain simulation at sensor location  $x_0 = 0.2 m$ 

### III. MODEL IDENTIFIABILITY ANALYSIS

In this combustion instability model, all variables can be either initially specified or measured directly from experiments except two parameters, the amplification factor  $\beta$  and time delay  $\tau$ , in the linear heat release model. Because the normalized transfer function magnitude depends on the two parameters, we can estimate of the two parameters with knowledge of the experimental transfer function magnitude from the time series pressure and particle velocity oscillations using the method in section II-E. However, due to the existence of measurement noise in practical experiments, there are statistical uncertainties in identifying the two parameters. In this section, we employ Fisher information analysis to evaluate the influence of experimental designs on this combustion instability model's identifiability.

# A. Fisher Information Analysis

Before performing the Fisher information analysis, we make a few assumptions. First, we assume that we know the input velocity oscillation exactly, although in real situations, the measurement of particle velocity oscillations also include noise. In addition, we assume an unbiased estimate of the parameter vector  $\theta$  that contains the parameters: amplification factor  $\beta$  and time delay  $\tau$ . Third, the analysis assumes Gaussian white noise w(x,s) in the pressure measurement, as indicated in (17). Fourth, each sample from the measurement of the observed transfer function is assumed to be independent and identically distributed so that each measurement has the same probability distribution  $p(|H_{n,m}(x,s)|;\theta)$  as the others and all are mutually independent. The subscript "m" in the transfer function indicates the measured observations. The equations (17) and (18) show the measured transfer function magnitude from experiments and the probability density function (PDF) for the observed objective. Function G describes the theoretical transfer function magnitude  $|H_n(x,s)|$ , which depends on the parameter vector  $\theta$ .

$$|H_{n,m}(x,s)| = G(x,s,\mathbf{\theta}) + w(x,s)$$

$$w(x,s) \sim \mathcal{N}(0,\sigma^2)$$
(17)

$$p(|H_{n,m}(x,s)|; \mathbf{\theta}) = \frac{1}{\sqrt{2\pi\sigma^2}} e^{-\frac{1}{2\sigma^2}[|H_{n,m}(x,s)| - G(x,s,\mathbf{\theta})]^2}$$
(18)

In (18), the PDF of the measured transfer function magnitude can also be viewed as the likelihood function for the unknown parameter vector  $\boldsymbol{\theta}$ . We expect a better estimate if  $\sigma^2$  is smaller. The expectation over the second derivative of the likelihood function at the true value of  $\boldsymbol{\theta}$  is one option for quantifying the "sharpness" of the function, which determines how accurately we can estimate the parameter. This expectation provides a lower bound for parameter estimate error variance, which is called the Cramér Rao lower bound (CRLB), as in equation (19). The denominator on the right hand side of (19) is referred to as Fisher information  $F(\boldsymbol{\theta})$ , which can also be expressed by the product of two first-order derivatives in (20) based on the third assumption.

$$\operatorname{var}(\hat{\boldsymbol{\theta}}) \geqslant \frac{1}{-E\left[\frac{\partial^{2} \ln p(|H_{n,m}|;\boldsymbol{\theta})}{\partial \boldsymbol{\theta}_{i} \partial \boldsymbol{\theta}_{j}}\right]}$$
(19)

$$\left[\boldsymbol{F}(\boldsymbol{\theta})\right]_{ij} = -E\left[\left(\frac{\partial \ln p(|H_{n,m}|;\boldsymbol{\theta})}{\partial \boldsymbol{\theta}_i}\right) \left(\frac{\partial \ln p(|H_{n,m}|;\boldsymbol{\theta})}{\partial \boldsymbol{\theta}_j}\right)^T\right]$$
(20)

# B. Optimization Scalar Objective - Fisher Information Matrix Determinant

In the combustion instability model, we define the parameter vector  $\theta$  in (21) with each parameter normalized by their nominal values; the definitions of nominal variables are in (22). The nominal flame flocation,  $b_0$ , is 0.25 m and the nominal bulk flow velocity,  $u_0$ , is 5 m/s.

$$\theta = \begin{bmatrix} \tau_n \\ \beta_n \end{bmatrix} \tag{21}$$

$$\tau_n = \frac{\tau}{\overline{\tau}}, \ \beta_n = \frac{\beta}{\overline{\beta}}$$

$$\overline{\tau} \equiv \frac{b_0}{u_0}, \ \overline{\beta} \equiv 1$$
(22)

Based on the normalized parameters, we achieve the Fisher information matrix (FIM), as illustrated in (23), with corresponding elements defined in (24).

$$F(\theta) = \frac{1}{\sigma^2} \begin{bmatrix} F_{11} & F_{12} \\ F_{21} & F_{22} \end{bmatrix}$$
 (23)

$$F_{11} = \sum_{i=1}^{N} \frac{\partial G_{j\omega_{i}}(x, s, \mathbf{\theta})}{\partial \tau_{n}} \cdot \frac{\partial G_{j\omega_{i}}(x, s, \mathbf{\theta})}{\partial \tau_{n}}$$

$$F_{12} = F_{21} = \sum_{i=1}^{N} \frac{\partial G_{j\omega_{i}}(x, s, \mathbf{\theta})}{\partial \tau_{n}} \cdot \frac{\partial G_{j\omega_{i}}(x, s, \mathbf{\theta})}{\partial \beta_{n}} \quad (24)$$

$$F_{22} = \sum_{i=1}^{N} \frac{\partial G_{j\omega_{i}}(x, s, \mathbf{\theta})}{\partial \beta_{n}} \cdot \frac{\partial G_{j\omega_{i}}(x, s, \mathbf{\theta})}{\partial \beta_{n}}$$

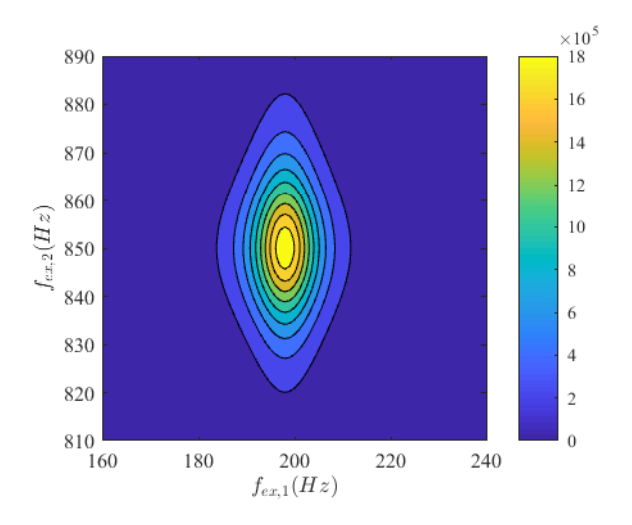


Fig. 4. Dependence of FIM determinant on two acoustic excitation frequencies  $f_{ex,1}$  and  $f_{ex,2}$ , with sensor placed at  $x_0 = 0.20$  m and flame located at b = 0.25 m

In equation (24),  $\omega$  is the acoustic excitation frequency and N is the number of the acoustic forcing frequencies. The covariance matrix  $C_{\hat{\theta}}$  representing the parameter estimate error variance is no smaller than the Fisher information matrix inverse, as expressed in (25).

$$C_{\hat{\theta}} \geqslant F^{-1}(\theta) = \frac{\sigma^2}{F_{11}F_{22} - F_{12}^2} \begin{bmatrix} F_{22} & -F_{12} \\ -F_{21} & F_{11} \end{bmatrix}$$
 (25)

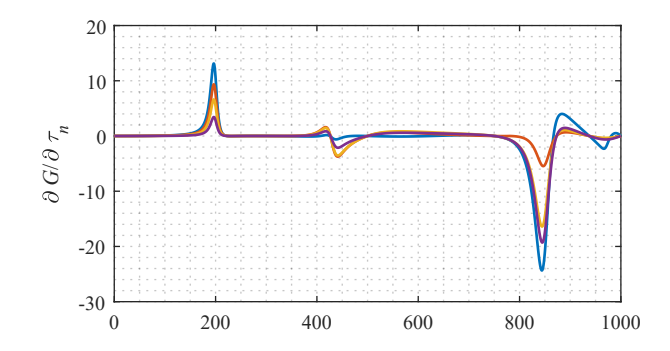
The goal of the parameter estimation accuracy improvement is equivalent to minimizing the two diagonal elements in the FIM inverse. Three design variables - flame location b, acoustic excitation frequency  $f_{ex}$ , and sensor placement  $x_0$  - affect the two diagonal elements in FIM inverse. Three optimal design techniques exist for simplifying the FIM to a scalar objective related to the shape of the uncertainty or confidence ellipsoids ([18], [19]). To minimize the overall variance of the two parameters estimate errors, we employ the D-optimal design technique in this work to minimize the area of the confidence ellipse, as defined in Equation (26), where the Fisher information matrix is calculated based on two excitation frequencies  $\omega_1$  and  $\omega_2$  since we need to estimate two unknown parameters.

$$det(\mathbf{F}) = \frac{1}{\sigma^4} \left( F_{11} F_{22} - F_{12}^2 \right)$$

$$= \frac{1}{\sigma^4} \left( \frac{\partial G_{j\omega_1}}{\partial \tau_n} \frac{\partial G_{j\omega_2}}{\partial \beta_n} - \frac{\partial G_{j\omega_2}}{\partial \tau_n} \frac{\partial G_{j\omega_1}}{\partial \beta_n} \right)^2$$
(26)

# IV. EFFECTS OF DESIGN VARIABLES ON FISHER IDENTIFIABILITY

Based on prior nominal values of the two parameters, amplification factor  $\beta$  and time delay  $\tau$ , in Table I, we analyze the dependence of the FIM determinant on the experimental design variables. The standard deviation of normalized transfer function magnitude measurement noise is assumed to be  $\sigma = 0.1$ .



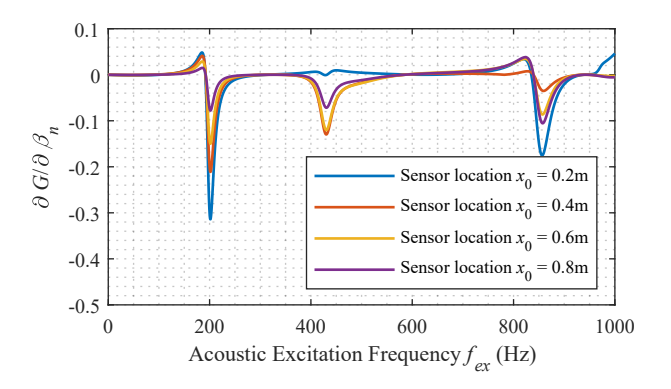


Fig. 5. Sensitivity of normalized transfer function magnitude with respect to normalized parameters at different acoustic forcing frequencies and four sensor locations with a flame located at b = 0.25 m

For one flame location, b = 0.25 m, one sensor placement, and  $x_0 = 0.2 m$ , Fig.4 illustrates the dependence of the FIM determinant on the two acoustic excitation frequencies  $f_{ex,1}$  and  $f_{ex,2}$  between 0 and 1000 Hz. The peak of the contour indicates the local maximum FIM determinant over the range of excitation frequencies ( $f_{ex,1}$ ,  $f_{ex,2}$ ); all the other local maxima were significantly smaller than the one shown here. The small region indicates that there is a strong dependence of the FIM determinant on two excitation frequencies.

# A. Dependence of FIM Determinant on Excitation Frequencies

As in (26), the FIM determinant is proportional to the absolute difference between the products of the normalized transfer function magnitude sensitivities with respect to the two normalized parameters at two excitation frequencies. In this section, we analyze the dependence of these sensitivities on the acoustic excitation frequency  $f_{ex}$  at four sensor placements  $x_0$  and one flame location b in Fig.5.

For all the four sensor placements, sensitivities with respect to normalized time delay,  $\tau_n$ , are approximately one order of magnitude larger than those with respect to the normalized amplification factor,  $\beta_n$ . This agrees with previous studies using the time-lag model [24] and thermoacoustic experiments ([25], [26]) that show a strong dependence of thermoacoustic instability on the time delay between the input disturbance and heat release oscillations. This result

indicates that experiments should be designed to minimize the uncertainty of  $\tau$ , even at the expense of the  $\beta$  estimation, given their disparate sensitivities. For all the four sensor placements, the sensitivities are greatest near the natural modes of the system. In addition, the dependence of the sensitivities on acoustic excitation frequency are similar for different sensor placements. This result is important for experimental design, as it means that the frequencies used to construct the optimal FIM determinant do not need to vary with sensor placement. Sharp peaks in the sensitivities for each sensor placement indicate that the FIM determinant is large over a small frequency range, which agrees with the contour plot in Fig.4. Sensor placement only significantly affects the sensitivities at the system natural modes.

## B. Dependence of FIM Determinant on Sensor Placement

Since the frequency dependence of the parameter sensitivities is not a strong function of sensor placement at a given flame location, the same excitation frequencies can be used to obtain the FIM for any sensor placement along the Rijke tube. The variation of the FIM determinant at a range of flame locations is shown in Fig.6. At any one of the flame locations, the FIM determinant varies along the spatial coordinate  $x_0$  nearly in a sinusoidal fashion. However, these variations are not sharp as compared to the variations with respect to excitation frequency in Fig.5. Sensors placed near the closed boundary end provide a larger FIM determinant than other locations. This initial result is partially encouraging, as the location with the highest determinant is not near and even upstream the flame, avoiding high heating load on the sensor.

# C. Dependence of FIM Determinant on Flame Location

When changing the flame location, the acoustic mode changes due to the variation of the temperature distribution in the system. As a result, the excitation frequencies need to be updated when calculating the FIM to ensure a maximum determinant. In contrast to the dependence on sensor placement, the FIM determinant varies significantly with flame location, as illustrated in Fig.6, where the flame is moved from  $0.05\ m$  to  $0.45\ m$ . The excitation frequency pairs for different flame locations are summarized in Table II.

 $\label{table ii} \textbf{TABLE II}$  Optimal excitation frequencies with flame at five locations

<i>b</i> (m)	0.05	0.15	0.25	0.35	0.45
$f_{ex,1}$ (Hz)	688 229.4	569.4	859.4	738.3	954.6
$f_{ex,2}$ (Hz)	229.4	216.5	199.2	178.4	157.9

Fig.6 illustrates the large difference between the FIM determinant at different flame locations. This strong sensitivity of the parameter estimation accuracy with respect to flame location suggests that optimal pressure sensor placement may be difficult to achieve in systems where the flame location is variable. As illustrated in Fig.7, when the flame location

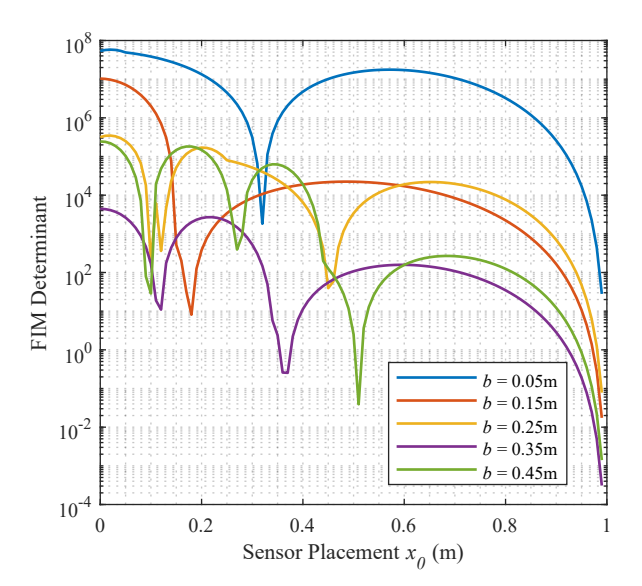


Fig. 6. Dependence of Fisher information matrix determinant on the flame location b

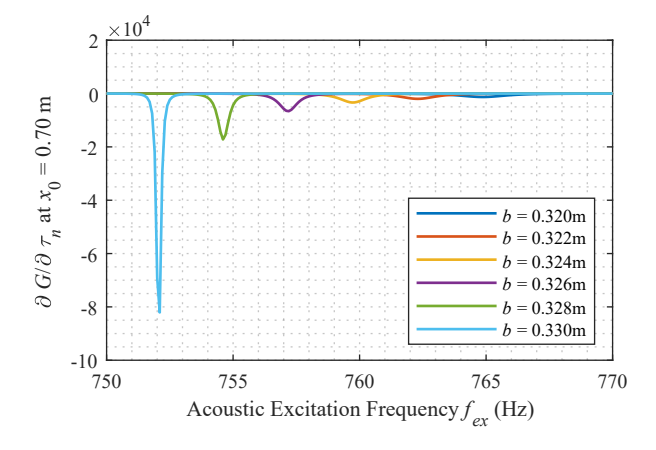


Fig. 7. Normalized time delay  $\tau_n$  sensitivity around a narrower frequency range with sensor placed at  $x_0 = 0.7$  m for six flame locations b

changes from 0.32 to 0.33 m, the strength of the third acoustic mode in the Rijke tube increases dramatically.

# V. OPTIMAL EXPERIMENTAL DESIGN

Based on the analysis in section IV, the model's parametric identifiability depends on flame location, acoustic excitation frequency, and sensor placement. A complete experimental design includes optimal values for these three variables. To obtain optimal model identifiability, we apply a genetic algorithm (GA) to optimize the sensor placement and two acoustic excitation frequencies by maximizing the FIM determinant. The optimization is conducted to find these values over a range of flame locations within the region [0.05L, 0.45L]. The excitation frequencies should be different by at least the minimum difference between resonant acoustic modes  $(m^{th}$  and  $n^{th})$  in the Rijke tube. As an additional constraint, the sensor should be placed at least  $0.05 \ m$  away from the flame to avoid heating load from the high

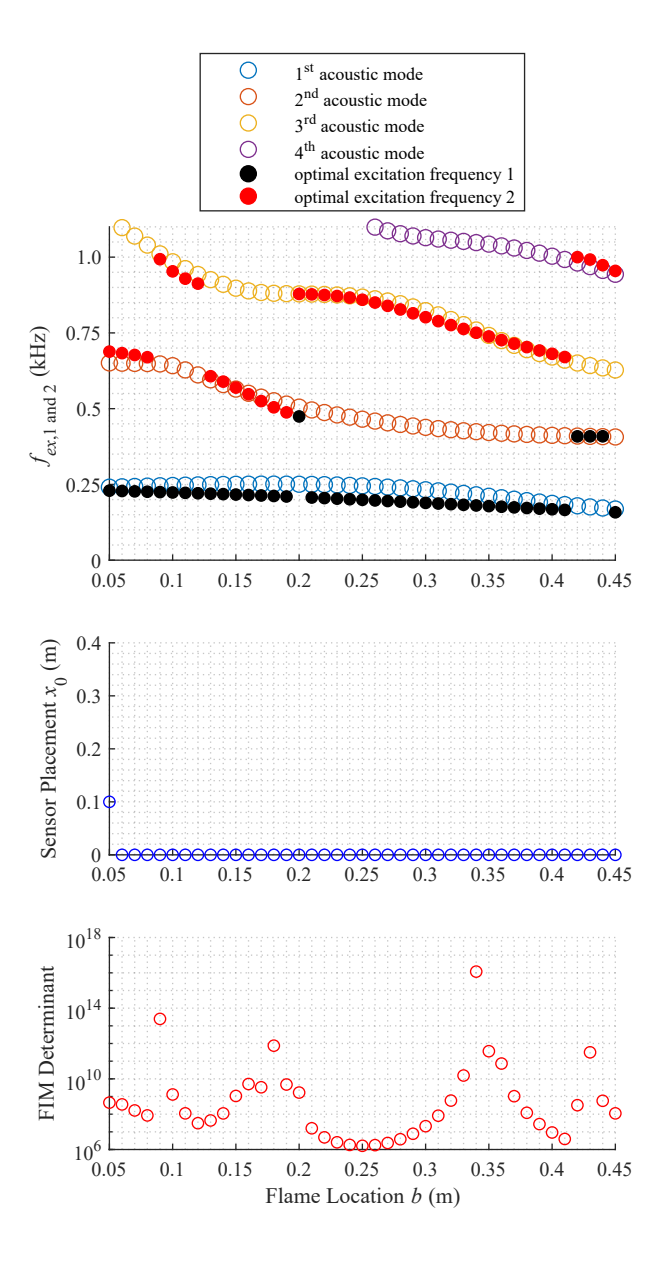


Fig. 8. Optimal experimental acoustic excitation frequencies for combustion instability model identifiability

temperature flame.

$$\det(\boldsymbol{F}) = \\ \mathbf{Max} \qquad \frac{1}{\sigma^4} \left( \frac{\partial G_{j\omega_1}}{\partial \tau_n} \frac{\partial G_{j\omega_2}}{\partial \beta_n} - \frac{\partial G_{j\omega_2}}{\partial \tau_n} \frac{\partial G_{j\omega_1}}{\partial \beta_n} \right)^2$$
 
$$\mathbf{Subject \ to} \qquad \omega = 2\pi f, \ 0 < f_{1,2} \leqslant 1000 \ Hz$$
 
$$|f_1 - f_2| \geqslant |f_m - f_n|_{min}$$
 
$$0 \leqslant x_0 \leqslant L, \ |x_0 - b| > 0.05 \ m$$

This optimization problem is non-convex, as seen in Fig.6, as the objective function is not smooth with respect to the sensor placement. To achieve the optimal experimental

design, we choose the genetic algorithm for global optimization. In the genetic algorithm, options are set as shown in III.

TABLE III

GENETIC ALGORITHM SETTING FOR MODEL IDENTIFIABILITY

OPTIMIZATION

Generation number	500
Population size	500
Crossover fraction	0.85
Crossover function	crossoverarithmetic
Selection function	selectionroulette
Function tolerance	0.001
Mutation function	mutationadaptfeasible

For each flame location, the GA algorithm returns two optimal acoustic excitation frequencies and one sensor placement for the thermoacoustic model identification experiment design. Fig.8 displays the design variable combination for each flame location. The optimal excitation frequencies (solid black and red circles) are close to the resonant modes (open circles) of the Rijke tube. The optimal sensor placements are mostly achieved at the combustor closed end where the pressure oscillation amplitude is high due to its proximity to the acoustic source and pressure anti-node position. For each flame location, the optimized FIM determinant achieves very different values, which agrees with the conclusion on the dependence of model identifiability on flame location in section IV-C.

### VI. CONCLUSIONS

This paper quantifies the uncertainty of the parameter estimate in a linear time-lag model that describes the dynamics between acoustics and heat release rate oscillations in a combustion system. The accuracy of the parameter estimation is quantified by the determinant of the Fisher information matrix. The FIM determinant is strongly dependent on the excitation frequencies and the flame locations, though not as sensitive to the location of the pressure sensors used to calculate the transfer function. With the current analysis, we can achieve the global optimized accuracy of the parametric identification when pressure oscillation measured near 0.00 m with two acoustic forcing frequencies near the first and third resonant modes and a flame located at 0.34 m. Optimization of the FIM determinant provides critical information for designing Rijke tube thermoacoustic model identification experiments.

#### **APPENDIX**

### A. Variable Definition in Pressure Solution Equations

$$\bar{\rho}_{m}\bar{c}_{m} = \bar{\rho}_{1}\bar{c}_{1} + (1 - \beta e^{-\tau s})\bar{\rho}_{2}\bar{c}_{2}$$

$$\bar{\rho}_{n}\bar{c}_{n} = \bar{\rho}_{1}\bar{c}_{1} - (1 - \beta e^{-\tau s})\bar{\rho}_{2}\bar{c}_{2}$$

$$\bar{\rho}\bar{c}e_{13} = \bar{\rho}_{m}\bar{c}_{m}e^{t_{1}s} + \bar{\rho}_{n}\bar{c}_{n}e^{t_{3}s}$$

$$\bar{\rho}\bar{c}e_{24} = \bar{\rho}_{m}\bar{c}_{m}e^{t_{2}s} + \bar{\rho}_{n}\bar{c}_{n}e^{t_{4}s}$$

$$e_{m} = e^{t_{1}s} + e^{t_{2}s}$$

$$e_{n} = e^{t_{3}s} + e^{t_{4}s}$$

$$t_{1} = \frac{b}{\bar{c}_{2}} + \tau$$

$$t_{2} = \frac{2b}{\bar{c}_{1}} + \frac{(2L - b)}{\bar{c}_{2}} + \tau$$

$$t_{3} = \frac{(2L - b)}{\bar{c}_{2}} + \tau$$

$$t_{4} = \frac{2b}{\bar{c}_{1}} + \frac{b}{\bar{c}_{2}} + \tau$$

$$t_{5} = \frac{b}{\bar{c}_{1}} + \tau$$

### ACKNOWLEDGMENT

This material is based upon work supported by the National Science Foundation under Grant No.e CMMI-1728307. Any opinions, findings, and conclusions or recommendations expressed in this material are those of the authors and do not necessarily reflect the views of the National Science Foundation.

### REFERENCES

- R. Raun, M. Beckstead, J. Finlinson, and K. Brooks, "A review of rijke tubes, rijke burners and related devices," *Progress in Energy and Combustion Science*, vol. 19, no. 4, pp. 313–364, 1993.
- [2] A. P. Dowling and S. R. Stow, "Acoustic analysis of gas turbine combustors," *Journal of Propulsion and Power*, vol. 19, no. 5, pp. 751–764, 2003.
- [3] K. Schadow, E. Gutmark, K. Wilson, and R. Smith, "Multistep dump combustor design to reduce combustion instabilities," *Journal* of Propulsion and Power, vol. 6, no. 4, pp. 407–411, 1990.
- [4] B. T. Zinn, "A theoretical study of non-linear damping by helmholtz resonators," *Journal of Sound and Vibration*, vol. 13, no. 3, pp. 347– 356, 1970.
- [5] J. Samarasinghe, W. Culler, B. D. Quay, D. A. Santavicca, and J. O'Connor, "The effect of fuel staging on the structure and instability characteristics of swirl-stabilized flames in a lean premixed multinozzle can combustor," *Journal of Engineering for Gas Turbines and Power*, vol. 139, no. 12, p. 121504, 2017.
- [6] Y.-T. Fung and V. Yang, "Active control of nonlinear pressure oscillations in combustion chambers," *Journal of Propulsion and Power*, vol. 8, no. 6, pp. 1282–1289, 1992.
- [7] G. Billoud, M. A. Galland, C. Huynh Huu, and S. Candel, "Adaptive active control of combustion instabilities," *Combustion Science and Technology*, vol. 81, no. 4-6, pp. 257–283, 1992.
- [8] A. P. DOWLING, "Nonlinear self-excited oscillations of a ducted flame," *Journal of Fluid Mechanics*, vol. 346, p. 271290, 1997.
- [9] A. M. Annaswamy, M. Fleifil, J. W. Rumsey, R. Prasanth, J.-P. Hathout, and A. F. Ghoniem, "Thermoacoustic instability: model-based optimal control designs and experimental validation," *IEEE Transactions on Control Systems Technology*, vol. 8, no. 6, pp. 905–918, 2000.
- [10] T. Poinsot, S. Candel, E. Esposito, W. Lang, and F. Bourienne, "Suppression of combustion instabilities by active control," *Journal of Propulsion and Power*, vol. 5, no. 1, pp. 14–20, 1989.

- [11] J. Hermann, A. Orthmann, S. Hoffmann, and P. Berenbrink, "Combination of active instability control and passive measures to prevent combustion instabilities in a 260mw heavy duty gas turbine," IfTA Ingenieurbuero fuer Thermoakustik GmbH, Siemens AG Power Generation, Tech. Rep., 2001.
- [12] F. Selimefendigil, R. Sujith, and W. Polifke, "Identification of heat transfer dynamics for non-modal analysis of thermoacoustic stability," *Applied Mathematics and Computation*, vol. 217, no. 11, pp. 5134– 5150, 2011.
- [13] S. Bittanti, A. De Marco, G. Poncia, and W. Prandoni, "Identification of a model for thermoacoustic instabilities in a rijke tube," *IEEE Transactions on Control Systems Technology*, vol. 10, no. 4, pp. 490– 502, 2002.
- [14] N. Noiray and B. Schuermans, "On the dynamic nature of azimuthal thermoacoustic modes in annular gas turbine combustion chambers," *Proceedings of the Royal Society A*, vol. 469, no. 2151, p. 2012.0535, 2013.
- [15] J. P. Epperlein, B. Bamieh, and K. J. Astrom, "Thermoacoustics and the rijke tube: Experiments, identification, and modeling," *IEEE Control Systems*, vol. 35, no. 2, pp. 57–77, 2015.
- [16] L. Crocco and S.-I. Cheng, "Theory of combustion instability in liquid propellant rocket motors," Princeton University NJ, Tech. Rep., 1956.
- [17] K. T. Kim, H. J. Lee, J. G. Lee, B. Quay, and D. Santavicca, "Flame transfer function measurement and instability frequency prediction using a thermoacoustic model." ASME Turbo Expo, 2009.
- [18] R. Mehra, "Optimal input signals for parameter estimation in dynamic systems-survey and new results," *IEEE Transactions on Automatic Control*, vol. 19, no. 6, pp. 753–768, 1974.
- [19] L. Pronzato, "Optimal experimental design and some related control problems," *Automatica*, vol. 44, no. 2, pp. 303–325, 2008.
- [20] S. Mosbach, A. Braumann, P. L. Man, C. A. Kastner, G. P. Brownbridge, and M. Kraft, "Iterative improvement of bayesian parameter estimates for an engine model by means of experimental design," *Combustion and Flame*, vol. 159, no. 3, pp. 1303–1313, 2012.
- [21] S. Mendoza, M. Rothenberger, A. Hake, and H. Fathy, "Optimization and experimental validation of a thermal cycle that maximizes entropy coefficient fisher identifiability for lithium iron phosphate cells," *Journal of Power Sources*, vol. 308, pp. 18–28, 2016.
- [22] A. Sharma and H. K. Fathy, "Fisher identifiability analysis for a periodically-excited equivalent-circuit lithium-ion battery model," Proceedings of the American Control Conference, pp. 274–280, 2014.
- [23] J. Li, D. Yang, C. Luzzato, and A. S. Morgans, "Open sounce combustion instability low order simulator (oscilos-long) technical report," 2015.
- [24] S. Ducruix, T. Schuller, D. Durox, and S. Candel, "Combustion dynamics and instabilities: Elementary coupling and driving mechanisms," *Journal of Propulsion and Power*, vol. 19, no. 5, pp. 722–734, 2003.
- [25] K. Venkataraman, L. Preston, D. Simons, B. Lee, J. Lee, and D. Santavicca, "Mechanism of combustion instability in a lean premixed dump combustor," *Journal of Propulsion and Power*, vol. 15, no. 6, pp. 909–918, 1999.
- [26] T. Lieuwen, H. Torres, C. Johnson, and B. T. Zinn, "A mechanism of combustion instability in lean premixed gas turbine combustors," *Journal of Engineering for Gas Turbines and Power*, vol. 123, no. 1, pp. 182–189, 1999.